Detection of hydrological variations and their impacts on vegetation from multiple satellite observations in the Three-River Source Region of the Tibetan Plateau

Min Xu [a,b], Shichang Kang [a,c,d,*], Xuelong Chen [c,b,**], Hao Wu [e], Xiaoyun Wang [f], Zhongbo Su [b]

[a] State Key Laboratory of Cryospheric Science, Northwest Institute of Eco-Environment and Resources, Chinese Academy of Sciences, Lanzhou 730000, China
[b] Faculty of Geo-Information Science and Earth Observation (ITC), University of Twente, Enschede 7513BH, Netherlands
[c] CAS Center for Excellence in Tibetan Plateau Earth Sciences, Chinese Academy of Sciences, Beijing 100101, China
[d] University of Chinese Academy of Sciences, Beijing 100049, China
[e] State Key Laboratory of Water Resources and Hydropower Engineering Science, Wuhan University, Wuhan 430072, China
[f] Key Laboratory of Western China's Environmental Systems (Ministry of Education), College of Earth and Environmental Sciences, Lanzhou University, Lanzhou 730000, China

HIGHLIGHTS

- The spatio-temporal variations of hydrological variables in the "Chinese Water Tower" were analyzed by multiple remote sensing data.
- The interactions of hydrological variables were discussed.
- The major determining factor for the vegetation in water budget was examined
- The effect of permafrost on TWS change were explored in vertical direction.

GRAPHICAL ABSTRACT
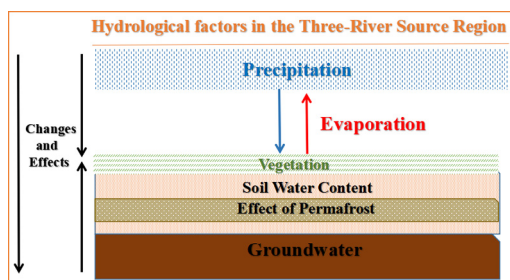
ABSTRACT

The Three-River Source Region (TRSR) of the Tibetan Plateau (TP) is regarded as the "Chinese water tower". Climate warming and the associated degradation of permafrost might change the water cycle and affect the alpine vegetation growth in the TRSR. However, the quantitative changes in the water budget and their impacts on the vegetation in the TRSR are poorly understood. In this study, the spatial-temporal changes in the hydrological variables and the normalized difference vegetation index (NDVI) during 2003–2014 were investigated using multiple satellite data and a remote sensing energy balance model. The results indicated that precipitation showed an increasing trend at a rate of 14.0 mm 10 a^{-1}, and evapotranspiration (ET) showed a slight decreasing trend. The GRACE-derived total water storage (TWS) change presented a significant increasing trend at a rate of 35.1 mm a^{-1}. The change in groundwater (GW) which showed an increasing trend at a rate of 18.5 mm a^{-1}, was estimated by water budget. The time lag of the GRACE-TWS that was influenced by precipitation was more obviously than was the GLDAS-SM (Soil Moisture) change. The vegetation in the TRSR was greening during the study period, and the accumulation of the NDVI increased rapidly after 2008. The effect of total TWS and GLDAS-SM on vegetation was considerably more than that the effects of other factors in this region. It was concluded that the hydrological cycle had obviously changed and that more soil water was transferred into the GW since the aquiclude changed due to climate warming. The increasing area and number of lakes and the thickening

---

* Correspondence to: S. Kang, State Key Laboratory of Cryospheric Science, Northwest Institute of Eco-Environment and Resources, Chinese Academy of Sciences, Lanzhou 730000, China.
** Correspondence to: X. Chen, CAS Center for Excellence in Tibetan Plateau Earth Sciences, Chinese Academy of Sciences, Beijing 100101, China.
E-mail addresses: shichang.kang@lzb.ac.cn (S. Kang), x.chen@itpcas.ac.cn (X. Chen).

of the active layer in the permafrost area led to the greater infiltration of surface water into the groundwater, which resulted in increased water storage.

1. Introduction

The Tibetan Plateau (TP), also called the "Asian Water Tower", is the highest and most extensive plateau in the world. More than one-sixth of the global population relies on the water supply from the TP (Immerzeel et al., 2010). With an abundant distribution of glaciers and permafrost, the TP is considered as one of the most sensitive areas to climate change in the world and the hydrological implications of climate change on the TP have become a global concern (Kang et al., 2010). Previous studies have indicated that the hydrological cycle in the TP has intensified and accelerated under recent climate change, which has also induced changes in the water balance (Huntington, 2006; Yang et al., 2011; Xue et al., 2013; Zhang et al., 2016a, 2016b). The hydrological control on the behavior of vegetation is obviously (Lewis et al., 2011). The TP is the most extensive alpine ecosystem in the world, and water is the primary resource limits vegetation activity; additionally, both climate change and hydrological variations have profound and significant impacts on vegetation changes in the TP (Piao et al., 2012; Gao et al., 2013; Zhang et al., 2016a, 2016b; Wang et al., 2016a, 2016b). Therefore, the research on hydrological variations and their influences on vegetation have been a key issue; furthermore, this information is helpful not only for understanding how the hydrological cycle responds to the climate change, but also for the evaluating the ecological environment and the management of water resources in alpine regions.

The Three-River Source Region (TRSR), which lies in the hinterland of the TP, constitutes an important part of the TP. As the "Chinese Water Tower", approximately 49% of the total water volume of the Yellow River, 15% of the volume of the Lantsang River, and a considerable amount of the volume of the Yangtze River volume originates from the TRSR (Xu et al., 2016). The region is a mosaic transition zone of seasonal frozen ground and areas of discontinuous and continuous permafrost (Luo et al., 2016). The TRSR has experienced significant climate warming in recent decades, and some permafrost has already degraded or disappeared (Liang et al., 2013; Cheng and Jin, 2013). Previous studies have indicated that regional climate change and permafrost degradation has altered the water balance at the regional scale (Yang et al., 2004; Ye et al., 2009; Woo et al., 2008; Gao et al., 2016), and variations in hydrology directly influenced vegetation (Roach et al., 2011; Jennifer et al., 2012; Walvoord et al., 2012). However, most research has focused on the trends of individual hydro-meteorological parameters in the TRSR. For example, Zhang et al. (2011) found that the discharge in the TRSR decreased, and no significant changes in precipitation occurred during 1965–2004. The evapotranspiration (ET) in the TRSR significantly decreased at a rate of 0.91 mm a^{-1} from 1980 to 2012, as calculated by the Penman-Monteith method (Wang et al., 2016a, 2016b). Other studies have focused on the relationships between climatological elements and runoff and ET in the TRSR. These results were all based on the analysis of point observations. The spatial-temporal quantitative changes in the water budget and the resulting impacts on the vegetation in the TRSR are still poorly understood. Conventional hydrological and climatic indicators, such as temperature and precipitation, have also been used to examine the hydrological control on vegetation by means of the normalized difference vegetation index (NDVI) in the TRSR (Hu et al., 2011; Xu et al., 2011). However, other components in the water cycle, such as changes in the terrestrial water storage (TWS), which includes changes in the soil water content and groundwater (GW), have been neglected. The main reason for this exclusion is that the monitoring of regional-scale changes in TWS change has been extremely limited, especially in remote areas. The change in TWS is essential for understanding a wide range of hydrological,

climatological, and ecological processes. In summary, the spatial-temporal changes in hydrological variables, e.g., precipitation, ET, TWS, soil water content and GW, have seldom been simultaneously discussed in the TRSR, specifically in terms of how hydrological variations impact vegetation.

In this study, the water balance and vegetation factors were analyzed using multiple satellite observations and a land surface model to unravel and quantify the spatial-temporal relationships among the climatological, hydrological and vegetation dynamics in the TRSR. The specific analyses the following: (1) changes in GW from 2003 to 2014 were estimated and evaluated using the GRACE satellite data and the Global Land Data Assimilation System (GLDAS) data using the water balance method. (2) The ET was estimated using the surface energy balance system (SEBS). (3) spatial-temporal variations in the hydrological variables and NDVI were analyzed. (4) The variation in the water cycle, i.e., the major determining factor influencing the vegetation, and the influence of permafrost on changes in the TWS in the TRSR were discussed. The purpose of this study was to reveal the changes in the water budget in a cryospheric region and to assess how the vegetation responds to changes in the hydrological conditions.

2. Study area

The TRSR, which is the source region of the Yangtze River, the Yellow River and the Lantsang River, is located in the central part of the TP (31°39′-36°16′N, 89°24′-102°23′E). The average elevation is 4200 m (rang: 3217–6575 m). The region has an area of 30.2×10^4 km^2 and includes the sub-regions of the individual sources of the Yangtze, Yellow, and Lantsang rivers, which cover 13.0×10^4, 11.8×10^4, and 5.4×10^4 km^2, respectively, and accounting for 43.2%, 39%, and 17.8% of the area, respectively. The average water flow out of the region is 1022.3 m^3 s^{-1} (Hu et al., 2011). The annual rainfall in the region is 498.9 mm, and the average annual temperature in the TRSR is 0.64 °C. Approximately 75% of the total precipitation occurs from June to September. The TRSR has a typical continental plateau climate, with strong radiation and cold, dry, and large diurnal variation in temperature (Wang et al., 2016a, 2016b). Most of the vegetation is alpine grassland and alpine steppe, and four types of permafrost are present in the TRSR: continuous permafrost, seasonal permafrost, island permafrost, and patchy permafrost, which encompass areas of 16.2×10^4, 12.0×10^4, 1.1×10^4, and 0.9×10^4 km^2, respectively (Fig. 1).

3. Dataset and methods

3.1. Dataset

3.1.1. Meteorological data

There are 18 national meteorological stations in the TRSR (Fig. 1), monthly temperature data from 2003 to 2014 were obtained from the National Climate Centre of China (http://ncc.cma.gov.cn). Other meteorological data used for the calculation of ET is downloaded from European Center for Medium-Range Weather Forecasts (ECMWF).

3.1.2. GRACE data

The TWS change is a key variable in the hydrological cycle. The Gravity Recovery and Climate Experiment (GRACE) satellite has provided data that can be used for analyzing the changes in TWS (Rodell et al., 2004; Syed et al., 2008; Yang et al., 2013; Strassberg et al., 2014; Cao et al., 2015; Long et al., 2016; Deng and Chen, 2016). In this study, the GRACE data were obtained from the University of Texas Center for
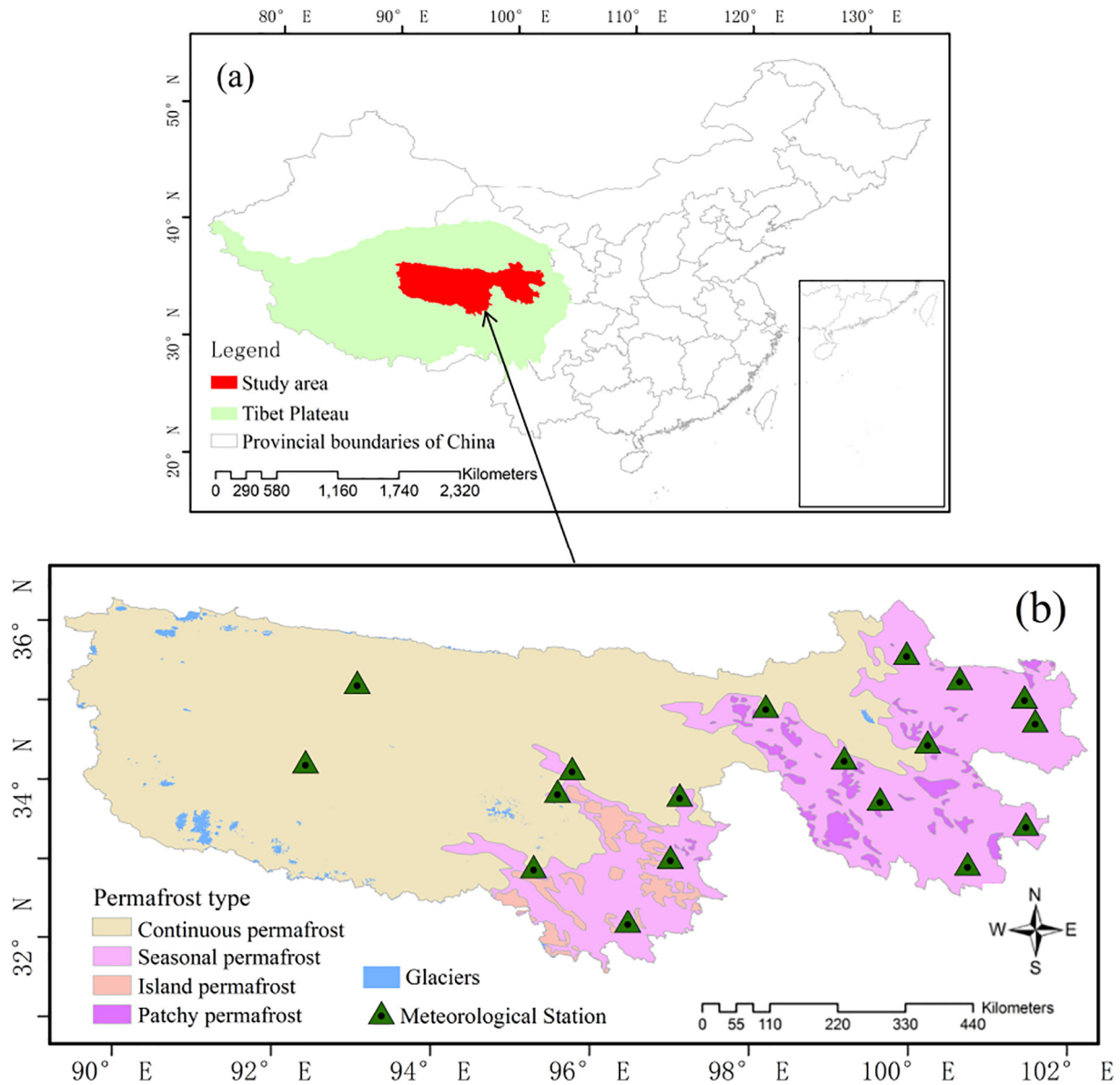
Fig. 1. Location of the Three-River Source Region (a), distributions of permafrost and meteorological stations in the study area (b).

Space Research (CSR) and can be freely downloaded from the GRACE Tellus website (http://grace.csr.nasa.gov/data/get-data/). We used the monthly time series of TWS for the period from 2003 to 2014. The data are presented spatially in 1° × 1° grid cells.

3.1.3. Soil and snow water content data

In this study, the data for soil moisture content and snow water equivalent came from the Global Land Data Assimilation System (GLDAS) Noah land surface model (http://disc.sci.gsfc.nasa.gov/services/grads-gds/gldas), which includes four-layer soil water contents for a soil depth of 2 m. The GLDAS data used here did not include GW but did include soil moisture (SM) and snow water equivalent (SWE); therefore, in addition to any errors in the model or observations, a difference from the GRACE-TWS changes can be expected. Additionally, the Greenland ice sheet areas have been masked out, as GLDAS does not currently feature a dynamic ice model; therefore simulated values over ice covered regions are not realistic (Rodell et al., 2004). The GLDAS data have a spatial resolution of 1° × 1° grid cells which is

consistent with the GRACE data. We used the monthly time series from GLDAS for the period ranging from 2003 to 2014.

3.1.4. Normalized difference vegetation index (NDVI) data

Moderate-resolution imaging spectroradiometer (MODIS) NDVI data from 2003 to 2014 were used to characterize changes in vegetation. The MODIS vegetation data (MOD13Q1, version-5) (Solano et al., 2010) was downloaded from the USGS (United States Geological Survey) website. Global MOD13Q1 data is provided every 16 days as a gridded level-3 product. The data was processed by image resampling with a spatial resolution of 0.1° × 0.1° (Wang et al., 2016a, 2016b). The growing season (May–September) of each year were extracted to analyze the changing trend of vegetation.

3.2. Methods

3.2.1. Method of GRACE retrieved TWS change

This study used GRACE Level-2 RL05 data from the University of Texas Center for Space Research. The current surface mass change data

are based on the RL05 spherical harmonics with an order of 60. The atmospheric pressure/mass changes were removed, and the C_{20} coefficients were replaced with the solutions from Satellite Laser Ranging (Cheng et al., 2011). Glacial isostatic adjustment (GIA) correction has been applied (Geruo et al., 2013). Correlated noises (N–S stripes) were removed from coefficients using a fifth-order polynomial that was fitted as a function for each odd or even set for a given order (Swenson and Wahr, 2006). Finally, a Gaussian averaging filter with a smoothing radius of 300 km was applied to calculate the TWS changes. These processed spherical harmonic coefficients were transformed into gridded data with 1-degree bins in the land grids. The global grids composed of 1-arc-degree water equivalent mass change were calculated by:

$$\Delta h(\phi, \lambda, t) = \frac{a_e \rho_e}{3\rho_w} \sum_{l=0}^{60} \sum_{m=0}^{l} \frac{(2l+1)}{1+k_l} W_l P_{lm} \, \sin(\phi) \\ \times [\Delta C_{lm}(t) \, \cos(m\lambda) + \Delta S_{lm}(t) \, \sin(m\lambda)] \tag{1}$$

$$Wl = \exp\left[\frac{(lr/a_e)^2}{4 \ln(2)}\right] \tag{2}$$

where Δh is the height of water equivalent (mm), P_{lm} is the normalized Legendre polynomials, $C_{lm}(t)$ and $S_{lm}(t)$ are the normalized time-varying Stokes spherical harmonic geopotential coefficients, a_e is the Earth's mean radius, r is the spatial radius, k_l are Love numbers, e is the Earth's mean density, β_w is the water density, t is the time, ϕ and λ are latitude and longitude, respectively.

Due to the sampling and post-processing of the GRACE observations, the surface mass variations that occur at small spatial scales tend to be attenuated. Therefore, the GRACE data should multiply the land data by the provided scaling grid. The scaling grid is a set of scaling coefficients, one for each 1-degree bin of the land grids, and the scaling coefficients are intended to restore much of the energy removed by the destriping, the Gaussian filter, and the degree-60 filter to the land grids (Landerer and Swenson, 2012).

3.2.2. ET from a remote sensing energy balance model

The monthly ET for 2000–2014 was delivered by using a recent enhanced surface energy balance system (SEBS) algorithm and MODIS satellite data (Chen et al., 2014a, 2014b, 2014c). The model was driven by remote sensing land surface temperature data and meteorological data. The ET was estimated using an energy balance method and aerodynamic parameterization formulas (Su, 2002; Chen et al., 2013). Evaluations showed that the revised model delivered better performance over bare soil, short canopy and snow cover on the Tibetan Plateau (Chen et al., 2013). The monthly mean land surface temperature (Chen et al., 2017) and the monthly mean air temperature, wind speed, pressure, and solar radiation were used to run the energy balance model at a monthly time step. The monthly mean sensible heat flux was derived from the difference between the monthly mean land surface temperature and the air temperature by using Monin–Obukhov similarity theory (Chen et al., 2014a, 2014b, 2014c). The monthly mean latent heat flux or ET was then estimated as the residual after the retrieval of the monthly mean net radiation and sensible heat (Chen et al., 2014a, 2014b, 2014c).

3.2.3. Estimation of GW using the water balance equation

The GRACE-observed data represents the total TWS changes (GRACE-TWS), including GW, snow, soil moisture, surface water and canopy water changes. The land surface total water storage is the summation of the snow, soil moisture, surface water, and canopy water from the GLDAS data. Therefore, the GW can be obtained after subtracting the GLDAS surface total water storage from the TWS derived from GRACE (Rodell et al., 2009; Jin and Feng, 2013). Previous studies found a good agreement between the GRACE estimated variations and the in situ observed groundwater variations (Feng et al., 2013; Chen et al., 2014a,

2014b, 2014c; Xiao et al., 2015; Long et al., 2016). The equation can be expressed as:

$$\Delta GW = \Delta TWS_{GRACE} - \Delta SM - \Delta SWE \tag{4}$$

where ΔGW is the groundwater change, ΔTWS_{GRACE} can be retrieved from the GRACE data, ΔSM and ΔSWE are the soil water content and snow water equivalent, respectively, which can be simulated from land surface hydrological models, herein, GLDAS.

3.2.4. Data masking for the study area

The spatial resolution of the GRACE/GLDAS data and the estimated GW are $1° \times 1°$ with a regular grid shape. However, the TRSR does not have a regular shape that matches with the grids of the data. Thus, the area from the intersection of GRACE/GLDAS and GW grid with the TRSR area was estimated. The intersection area represents the amount of area in the grid. Additionally, a weight was given to the region area to mask the GRACE/GLDAS and GW grid. The weight and estimation of GRACE/GLDAS and GW are followed by:

$$W_i = \frac{a_i}{g_i} \\ V_N = \frac{\sum_{i=1}^{n}(v_i * w_i)}{A} \tag{3}$$

where W_i is the weight of grid i; a_i is the area of the region in grid i with the GRACE/GLDAS data and GW grid; g_i is the area of the $1° \times 1°$ GRACE/GLDAS and GW grid cell; V_N is the value of data for the entire region for month N; v_i is the value the data of grid i; A is the total area of the TRSR; and n is the number of the GRACE/GLDAS and GW grids.

3.2.5. Spatial trends of hydrological variables and NDVI

A univariate linear regression method was used to analyze the spatial trends in the hydrological variables and NDVI, which used the time and factors as the independent and dependent variables, respectively (Wang et al., 2011). The slope of the linear regression was used to illustrate the trend. We calculated the inter-annual slope using the following equation:

$$slope = \frac{12 \times \sum_{i=1}^{12} i \times a_i - \left(\sum_{i=1}^{12} i\right)\left(\sum_{i=1}^{12} a_i\right)}{12 \times \sum_{i=1}^{12} i^2 - \left(\sum_{i=1}^{12} i\right)^2} \tag{5}$$

where *slope* is the trend, a_i is the value of annual hydrological variables or NDVI in each grid, and i represents the year, e.g., 2003 was the first year, 2004 was the second year, and so on. A positive slope indicates an increasing trend, and a negative slope indicates a decreasing trend.

4. Results

4.1. Annual distributions of hydrological factors

Fig. 2 shows the seasonal distributions of precipitation, ET, GRACE-TWS change, GLDAS-SM (soil moisture) change and GW change in the TRSR during 2003–2014. The precipitation and ET mirrored each other fairly well, with both variables exhibiting higher values during the summer and lower values during the winter. In the TRSR, increases in the GRACE-TWS were concentrated mainly from June to December, and negative values were observed during other months. The peaks of the GRACE-TWS change was 33.6 mm in September, and the lowest value reached in April with a seasonal amplitude of −19.3 mm. Conversely, the SM simulated by GLDAS showed positive values from January to July and in October, but the values were negative during the other months; furthermore, the maximum and minimum value were 15.2 mm (June) and −1.4 mm (December), respectively. Generally, the GRACE-TWS change was higher in summer and autumn and lower
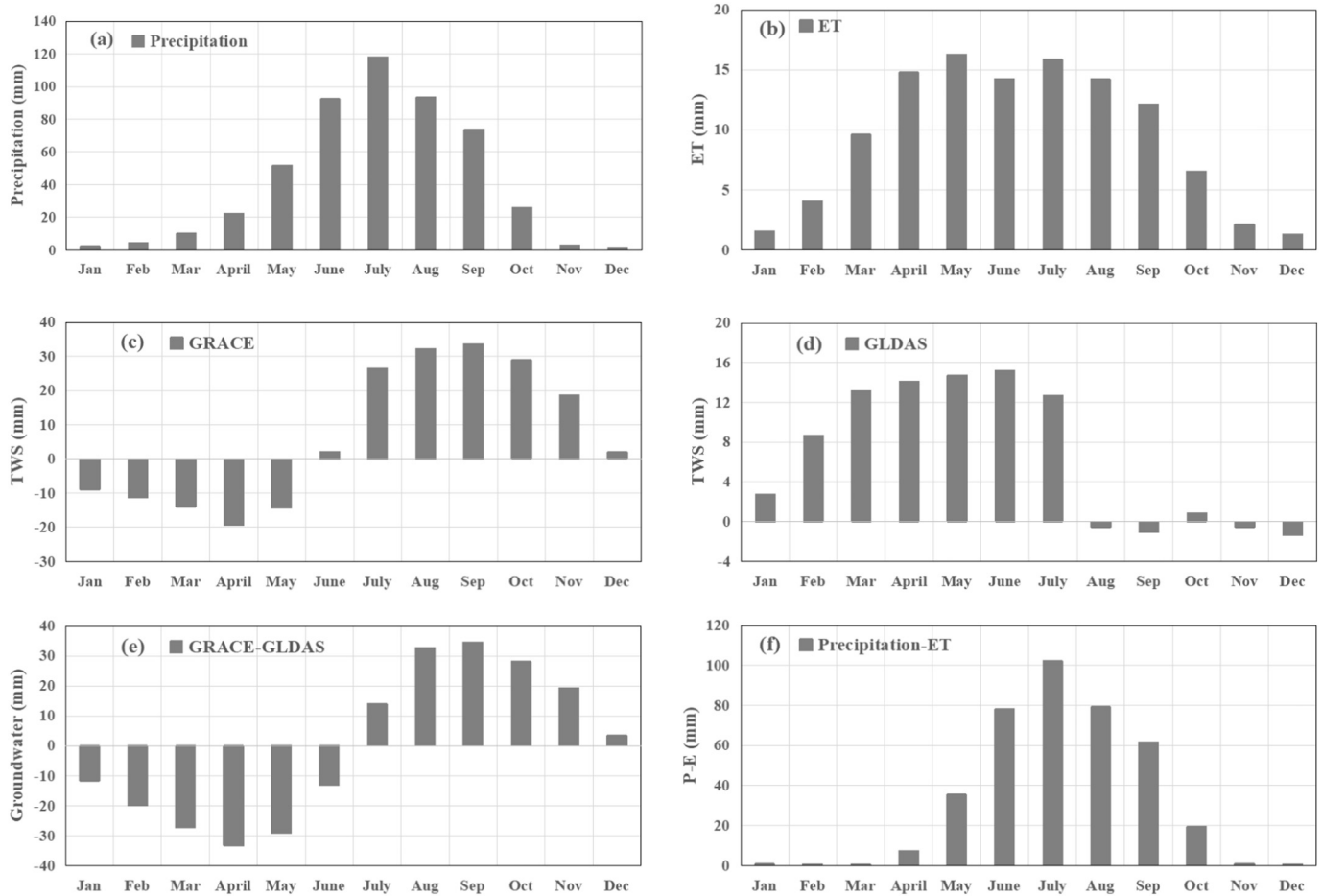
Fig. 2. Monthly distributions of averaged hydrological factors ((a) precipitation; (b) ET; (c) GRACE-TWS change; (d) GLDAS-SM change; (e) GW change and (f) P-E) in the TRSR during 2003–2014.

in winter and spring. Precipitation was relatively lower in winter and spring, and the water flow out of the TRSR was predominantly in the forms of ET and discharge which led the TWS in a state of loss. The monthly GW change calculated by GRACE-GLDAS and GRACE-TWS change showed similar seasonal cycles but were distinct in terms of precipitation and ET. It was clear that the water was mainly stored as SM from January to July, but then a change occurred, and water was stored as GW change from July to December in the TRSR. The relatively more abundant rainfall in July contributed to a higher magnitude to GLDAS-SM change and GW change in the study area. The differences between the monthly precipitation and the monthly ET were high from June to September and low in the winter and spring (Fig. 2f).

4.2. Annual spatial distributions of hydrological factors in the TRSR

The spatial distributions of the average annual precipitation, ET, GRACE-TWS change, GLDAS-SM change and GW change in the SRTR are shown in Fig. 3a–e, respectively, for the period of 2003–2014. The values of annual average precipitation, ET, GRACE-TWS change, GLDAS-SM change and GW change were 498.9 mm, 111.8 mm, 76.3 mm, 78.6 mm and −2.3 mm, respectively. The total TWS change represented in a state of gain; however, the GW change represented a state of loss from 2003 to 2014. Additionally, precipitation was higher in the eastern part of the SRTR than in the western part of the SRTR. The spatial distribution of ET was consistent with that of precipitation. There were differences between the spatial distributions of GRACE-TWS change and precipitation, which indicated that the distribution of TWS change was not only influenced by precipitation, but also may have been affected by the types of underlying surfaces

(i.e., permafrost and lakes). The GRACE-TWS change was in a state of surplus in most regions with continuous permafrost areas (Figs. 1b and 3c). There were numerous and quite large thawed ponds, lakes, and drained thawed-lake basins in the areas of continuous permafrost in the SRTR (Zhang et al., 2017). The development and growth of lakes was related to the thermal processes at the ice-wedge intersections, the permafrost thawing with subsidence of the ground surface, and the increased thickness of the active layer (Muskett and Romanovsky, 2011). Beneath these lakes, the talik that was previously unfrozen soil developed into a closed talik, and the lateral and vertical extents of the talik depended on the internal structure of the permafrost and the temperature regime at the ground surface. A talik can become an open talik and serve as an aquifer and this leads to increases of the TWS in this area. The GLDAS-SM change showed the highest gains in the west, while the lowest value occurred in the east; moreover, most of the middle part of the SRTR was in a state of loss. However, the positive changes in GW were mainly concentrated in the middle of the SRTR.

4.3. Time series analysis of temperature and hydrological variables

The time series of the temperature and hydrological components showed distinct annual fluctuations in the TRSR during the period of 2003–2014 (Fig. 4). The temperature increased with the annual fluctuations from 2003 to 2014. The average temperature rate of increase rate was 0.11 °C 10 a^{-1} in the TRSR. Compared with the trend before 2010, a rapid decrease in the annual mean temperature occurred after 2010. The annual precipitation increased with fluctuations from 2003 to 2014 in the TRSR. The average precipitation rate of increase was 14.0 mm 10 a^{-1}. A rapid increase in the annual mean precipitation
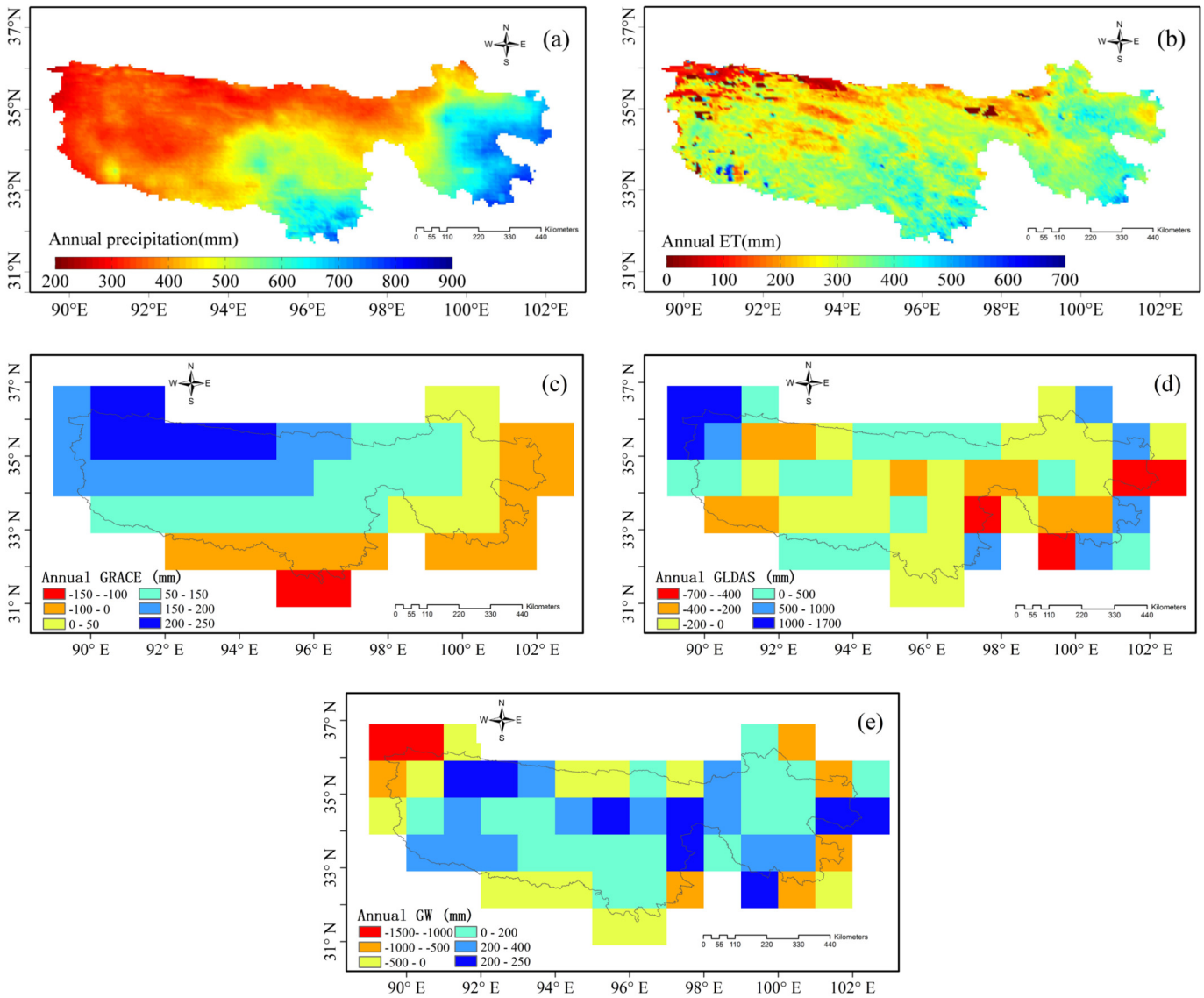
Fig. 3. Spatial distribution of average annual ((a) precipitation, (b) ET, (c) GRACE-TWS change, (d) GLDAS-SM change and (e) GW change) in the TRSR during 2003–2014.

occurred after 2006. The annual ET decreased at a rate of 3.3 mm 10 a^{-1}. The previous study indicated that decreases in net radiation, wind speed, and actual vapor pressure had positive effects in terms of decreasing ET (Wang et al., 2016a, 2016b). Both GRACE-TWS and GLDAS-SM showed increasing trends during 2003–2014, at rates of 35.1 mm a^{-1} and 16.6 mm a^{-1}, respectively. During 2003–2014, the GW showed an increasing trend at a rate of 18.5 mm a^{-1}, which suggested that more water was stored underground. It has become rather clear, that during the study period, the GW was stable before 2009, but it experienced a significant increase afterwards. The largest yearly GW depletion occurred in 2009. These results suggested that the increase in GRACE-TWS mainly consisted of increases in GLDAS-SM and GW in the SRTR.

The four seasons were defined as spring (March to May), summer (June to August), autumn (September to November) and winter (December to February). The seasonal analysis results indicated that there were seasonal differences in the hydrological variations in the TRSR during the 12-year study period (Fig. 5). The precipitation showed increasing trends in spring, summer and autumn, and it had a slightly negative anomaly in winter. The highest and lowest positive trends occurred in autumn (8.3 mm 10 a^{-1}) and summer (1.4 mm 10 a^{-1}), respectively. The ET showed a slight increasing trend in spring (1 mm 10 a^{-1}) and autumn (0.5 mm 10 a^{-1}), and a slight decreasing trend in summer

(-3.7 mm 10 a^{-1}) and winter (-1.1 mm 10 a^{-1}). The GRACE-TWS change had a positive anomaly in all four seasons, with the highest and lowest positive trends occurring in autumn (10.5 mm a^{-1}) and summer (7.6 mm a^{-1}), respectively. The increasing GLDAS-SM change ranged from 1.0 mm a^{-1} to 7.9 mm a^{-1}, and the lowest and highest positive trends occurred in autumn and spring, respectively. The increasing magnitudes of the GW change trend were 0.6 mm a^{-1}, 6.5 mm a^{-1}, 6.6 mm a^{-1} and 4.8 mm a^{-1} for spring, summer, autumn, and winter, respectively. Fig. 5 presents the trend of GW change that exhibited a variation that fluctuated with season, producing a "saddle shape", and the GLDAS-SM change showed a converse shape with the state of the GW. These results suggested that the process of water migration was from the soil water content to the GW during these seasonal alternations. The seasonal trend of the hydrological variation indicated that the capacity of water storage in the SRTR increased in recent years, especially in summer, and more water was stored in the study area.

4.4. Spatial annual trend of hydrological variables in the TRSR

The trends of the hydrological variables were calculated using Eq. (5). The overall results revealed that the annual precipitation increased over most of the TRSR during 2003–2014 (Fig. 6a). The highest
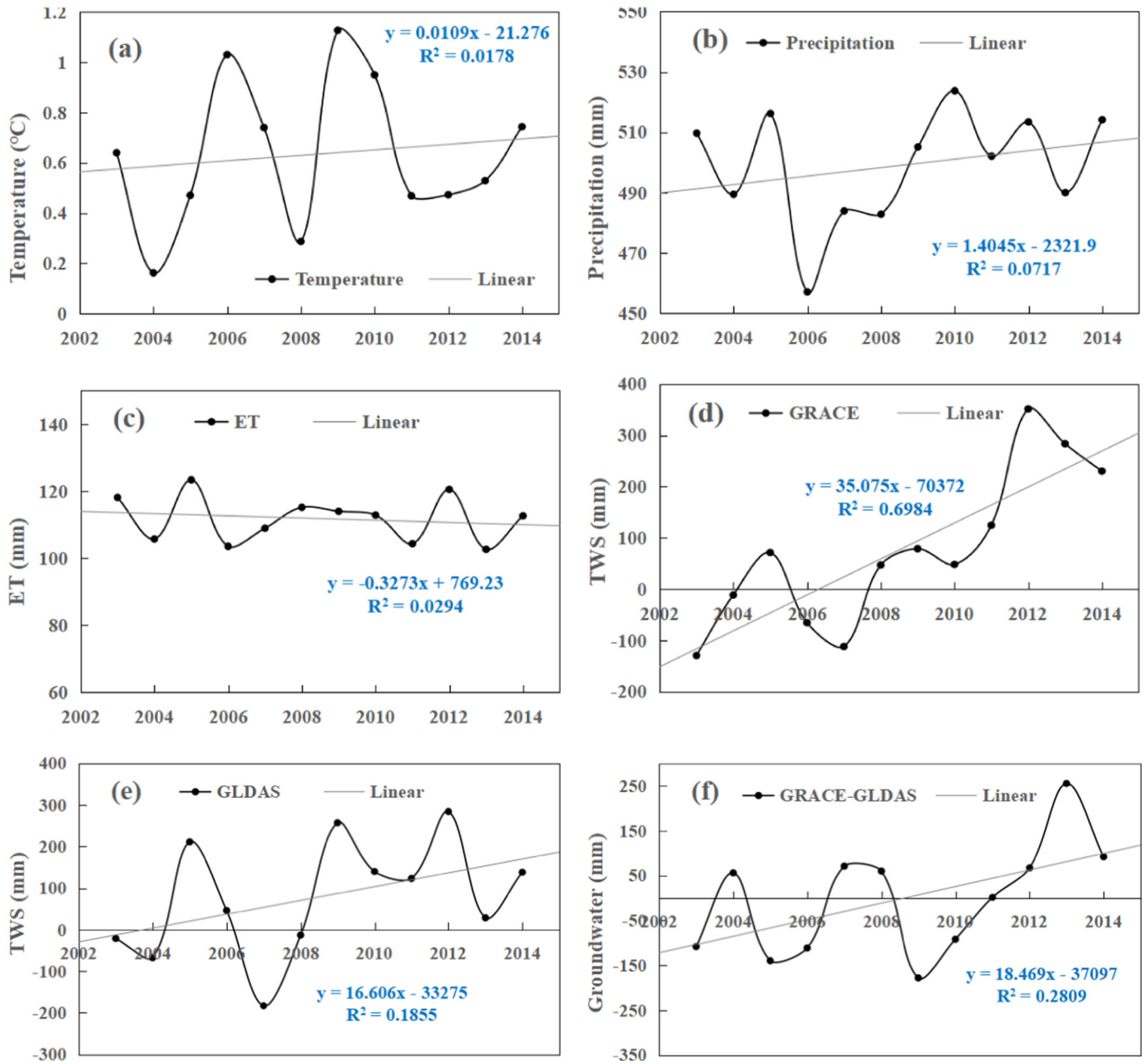
Fig. 4. Temporal variability of temperature (a) and hydrological variables ((b) precipitation; (c) ET; (d) GRACE-TWS change; (e) GLDAS-SM change and (f) GW change) in the TRSR during 2003–2014.
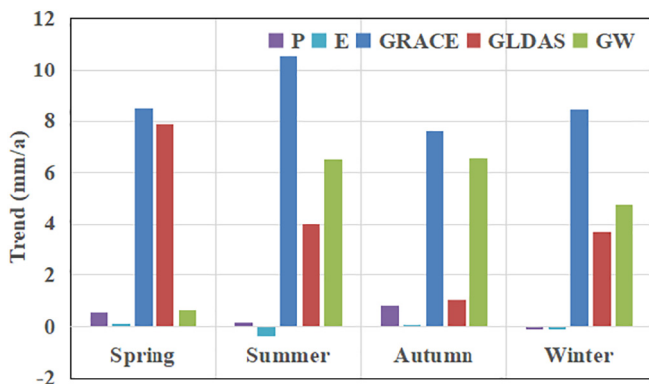

Fig. 5. Seasonal hydrological variations in the TRSR during 2003–2014.

increasing trend in annual precipitation was concentrated in the area with continuous permafrost, where the annual precipitation was lower. However, the annual precipitation decreased in a small portion of the eastern TRSR as well as in middle and western parts of the study area. The ET showed a decreasing trend in the eastern part of the TRSR, and it increased in most parts of the middle and western study area. There was a positive trend for GRACE-TWS in most parts of the TRSR, and the trend decreased from the west to the east and from the north to the south. The GLDAS-SM showed a decreasing trend for most parts of the TRSR, especially in the area with continuous permafrost. The increasing trend in GLDAS-SM mainly appeared in the peripheral regions of the study area, and the soil became drier overall. The distribution of the spatial trend for GW contrasted with that from GLDAS-SM. The GW in most parts of the TRSR showed an increasing trend. As seen, the spatial distribution of the increasing trend in
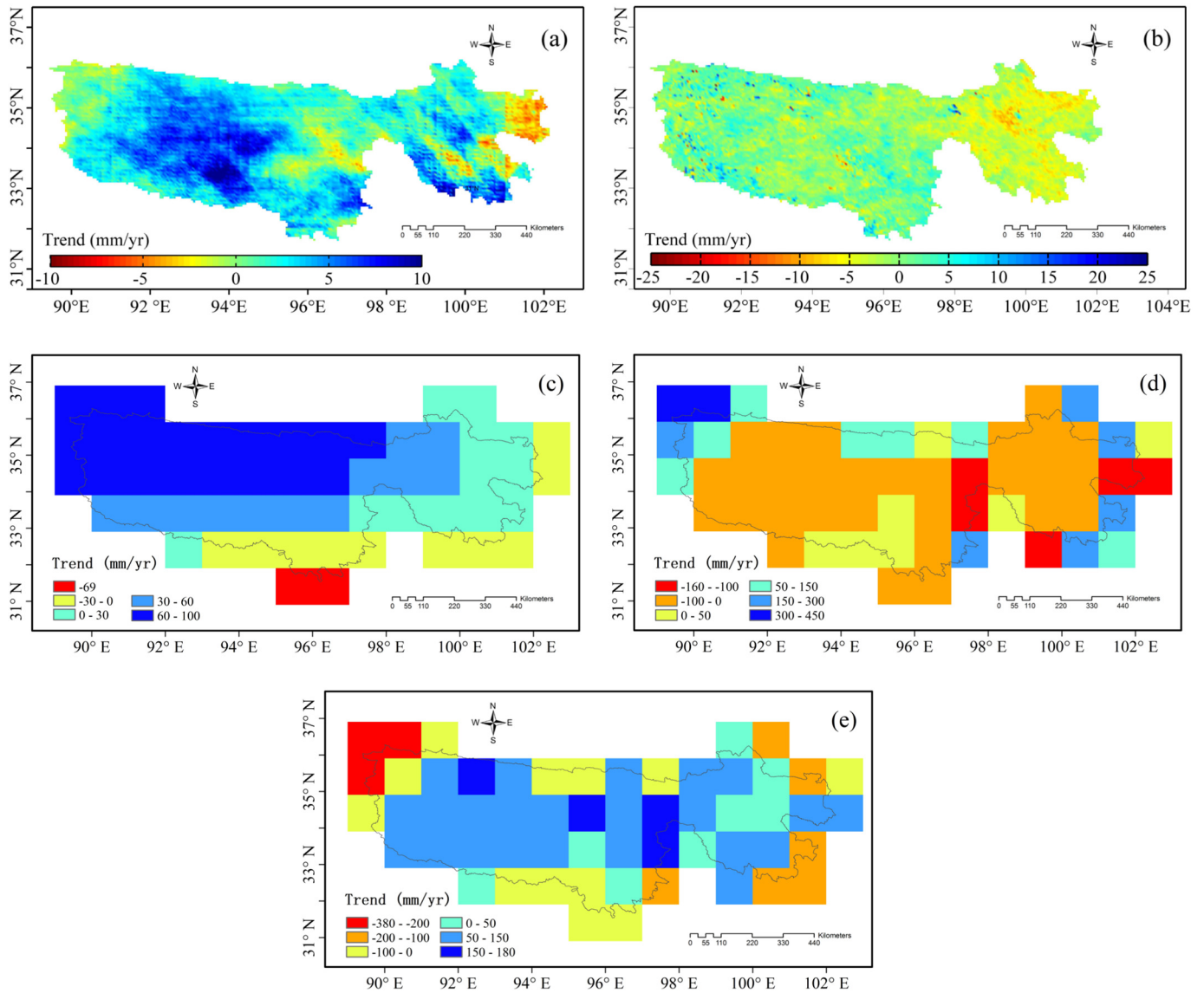
Fig. 6. The trend of hydrological variations (a) precipitation; (b) ET; (c) GRACE-TWS change; (d) GLDAS-SM change and (e) GW change in the TRSR during 2003–2014.

precipitation was consistent with the GRACE-TWS and GW, but contrasted with that of GLDAS-SM. However, the changes in precipitation and ET were far below those for GRACE-TWS, GLDAS-SM and GW. The results indicated that more water was stored in the TRSR during 2003–2014, and more soil water has been transported into GW since the aquiclude changed due to global warming.

4.5. Spatial-temporal variations of NDVI in the TRSR

Surface vegetation is a sensitive indicator of the hydrological cycle, and previous studies have indicated the importance of hydrological control on vegetation behavior (Ye et al., 2012; Shen et al., 2015). Based on the MODIS NDVI data for the TRSR from 2003 to 2014, this study systematically analyzed the temporal change pattern and accumulative NDVI during the annual growing seasons (Fig. 7a). The results indicated that the vegetation in the TRSR was greening between 2003 and 2014. The linear trend estimation method showed that the NDVI increased from 2003 to 2014 at a rate of 0.03 decade^{-1}. This is consistent with a previous study that showed a positive trend from 1982 to 2010 (Zhang et al., 2010). The annual accumulated NDVI anomalies in the TRSR indicated that the changes in NDVI varied in the different periods (Fig. 7b). The accumulated NDVI anomalies decreased rapidly from

2003 to 2008 and increased rapidly from 2008 to 2014. The annual mean NDVI and the variation trend of the NDVI in the TRSR during 2003–2014 are shown in Fig. 8. The spatial patterns of the NDVI in the growing season were heterogeneous. Most areas with an NDVI < 0.2 were found in the north-western part of the TRSR; additionally, the areas with 0.2 < NDVI < 0.6 were located in the middle of the TRSR, and the areas with an NDVI > 0.6 were in the south-eastern area. The spatial distribution of the NDVI was seen to be quite relative in terms of the climate and hydrological variations. The trend of the NDVI indicated that 90% of the TRSR areas had a positive annual variation rate, while the negative rate found in the other areas corresponded to degraded vegetation. The areas where vegetation was worsening were located in parts of the eastern, southern, and western TRSR.

5. Discussions

5.1. The interactions among hydrological variables

Precipitation is the key variable in the water budget, and it is also the most influential factor that affects interactions among the hydrological cycle (Gao et al., 2014). There is a lag time from when the water is introduced as rainfall to when it becomes surface water and groundwater. In
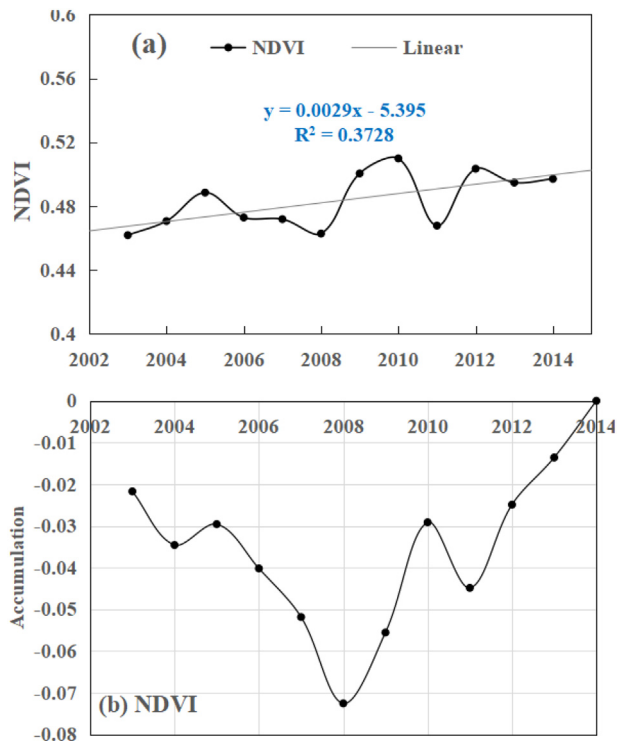
Fig. 7. Inter-annual variations (a) and curve of accumulation (b) in NDVI on the growing season timescales for 2003–2014 in the TRSR.

most hydrological forecasting, the lag time is typically described empirically using total precipitation that is in hydrological balance (Thompson et al., 2011). The different monthly time lags of the GRACE-TWS and GLDAS-SM responses to precipitation and the P-ET (subtract ET from precipitation) were analyzed in the TRSR. The results indicated that the GRACE-TWS change anomalies were highly related to precipitation over a time-lag of 2 months, i.e., the monthly total TWS was strongly influenced by the precipitation that occurred two months earlier (Fig. 9a). The co-relationships between the monthly precipitation and the GLDAS-SM change were more complicated; specifically, this relationship was poorly positively correlated over a 0-month lag and was strongly negatively correlated over a 3-month lag (Fig. 9a). These results suggested that more precipitation would lead to more GRACE-TWS changes when precipitation preceded GRACE-TWS changes by 2 months; in contrast, it would induce less GLDAS-SM change when precipitation preceded it by 3 months. The result of P-ET showed a positive correlation with GRACE-TWS change over a 0-month lag; however, these two variables had the highest negative correlation over a 4-month lag. The highest correlation between GLDAS-SM change and P-E was obtained over a 2-month lag. In the TRSR, the time lag of the GRACE-TWS change that was influenced by precipitation was more obvious than was the GLDAS-SM change in the TRSR. No consistent changes in correlation between hydrological variables were found with the increase in the time-lag.

The correlation between the annual GRACE-TWS change, the GLDAS-SM change and the precipitation were calculated in the TRSR (Fig. 10). The changes in annual precipitation were more highly related to changes in the GLDAS-SM than to changes in the GRACE-TWS (Fig. 10a and b), with correlation coefficients of 0.570 and 0.372, respectively. The GLDAS-SM was primary driven by precipitation variations, increased precipitation led to increased soil water during 2003–2014. However, the annual GRACE-TWS change was more dependent on the P-ET. The GLDAS-SM change had a weaker correlation with the P-ET. The changes in annual GLDAS-SM had a positive correlation with the changes in GRACE-TWS, as more soil water content often meant more

total TWS. Therefore, the annual precipitation had the greatest impact on the surface water (GLDAS-SM). The annual precipitation and ET affected the total water storage change (GRACE-TWS) which also responded to GLDAS-SM change in the TRSR.

5.2. Impacts of temperature and hydrological variables on NDVI

Climate has an inevitable impact on the growth environment and on the condition of vegetation (Chen et al., 2014a, 2014b, 2014c). Conventional hydrological indicators, such as precipitation and soil moisture, have been widely used to examine the hydrological controls on terrestrial ecosystems (Ye et al., 2012; Shen et al., 2015). To further understand the impacts of temperature and hydrological variables on NDVI during the growing season, we examined the relationships between NDVI and temperature and four hydrological variables (precipitation, ET, GRACE-TWS change and GLDAS-SM change) in the TRSR for the period from 2003 to 2014 (Table 1). The average NDVI of the growing season in the TRSR was significantly correlated with the summer temperature; however, it was only very weakly correlated with the temperature in other seasons. The results suggested that the response of vegetation to temperature in high-cold regions was likely to be more intense under climate warming. The spring precipitation was positively correlated with the NDVI, which reached a confidence level of 99%. Spring precipitation may not directly support vegetation growth in the current season (as reflected by the NDVI), but the relationship was affected by the time lag of the response of vegetation to precipitation. The ET did not show an obvious relationship with the NDVI. The NDVI was significantly positively correlated with the GRACE-TWS change and GLDAS-SM change during the growing season (except for autumn), and the highest values occurred in winter and summer, respectively. This result can be explained by the fact that the GRACE-TWS in winter provided sufficient water storage for the growth of vegetation during the growing season, and the roots of the vegetation were strongly dependent on surface soil moisture conditions in summer, which provided the water available for plants. The relationships between NDVI and precipitation were much weaker than those between NDVI and GRACE-TWS change and GLDAS-SM change. This result indicated that seasonal variability in surface greenness over the TRSR was also controlled by changes in other hydrological conditions, and GRACE-TWS change and GLDAS-SM change appeared to be better hydrological indicators for explaining variability in vegetation dynamics than was precipitation. This result is reasonable because precipitation provides only an indirect measure of water availability for plant growth. Spring precipitation and summer temperature were the limiting conditions affecting vegetation growth, and precipitation was more influential than temperature. However, the effects of total TWS change and GLDAS-SM change on vegetation were more pronounced than were other factors in this region.

5.3. Effects of permafrost on hydrological regime

The distribution of permafrost is extensive in the TRSR, and these areas are highly sensitive to temperature change. Significant soil warming was detected during 1981–2014, at rates of 0.71 °C 10 a^{-1} for surface soils (0 cm), 0.48 °C 10 a^{-1} for shallow layer soils (5–20 cm) and 0.42 °C 10 a^{-1} for deep layer soils (40–320 cm) (Luo et al., 2016). Due to the influence of climate warming, permafrost has been degrading extensively, with marked spatial-temporal variability over the last 30 years (Cheng and Jin, 2013). The number of permafrost thawing days and the thickening of the permafrost active layer have increased (Yang et al., 2010; Song et al., 2018). In the cold regions, the hydrological regimes are closely related with permafrost conditions, such as the extent of permafrost and the thermal characteristics; additionally, the hydrological regimes are controlled by the distribution of frozen ground and taliks as well as by the freeze-thaw processes of aquifers (White et al., 2007; Ye et al., 2009; Song et al., 2018). As a special
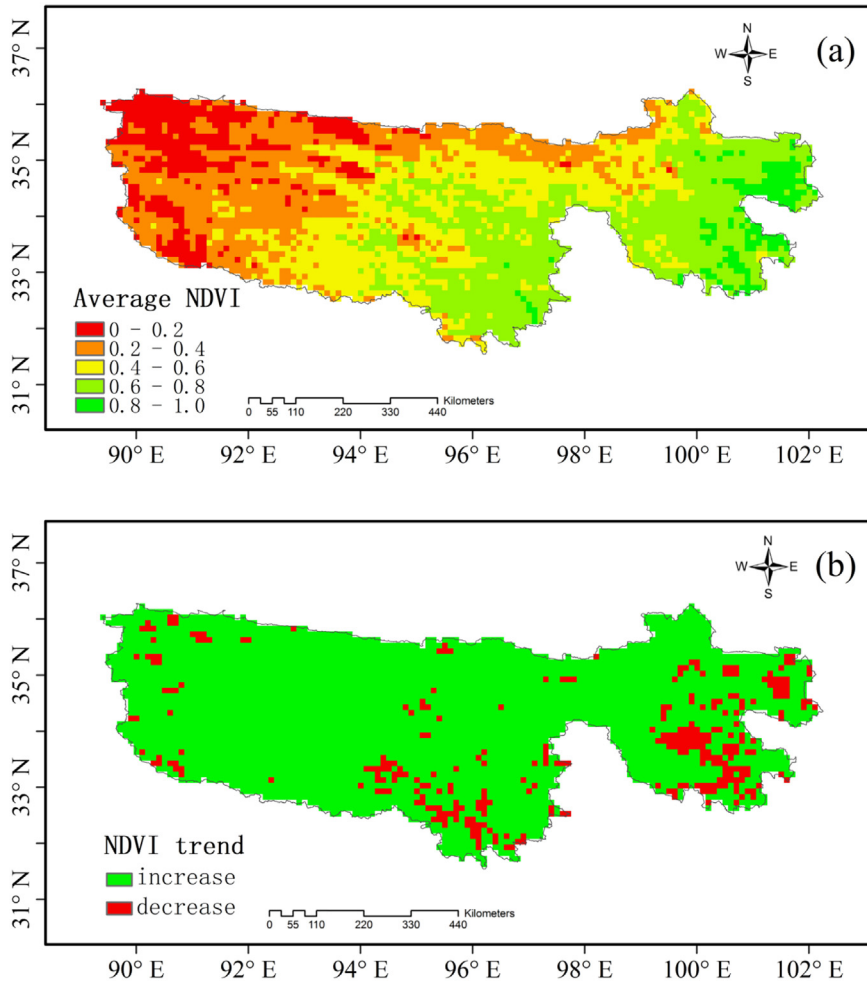
Fig. 8. Annual mean NDVI and variation trend of NDVI in the TRSR during 2003–2014.
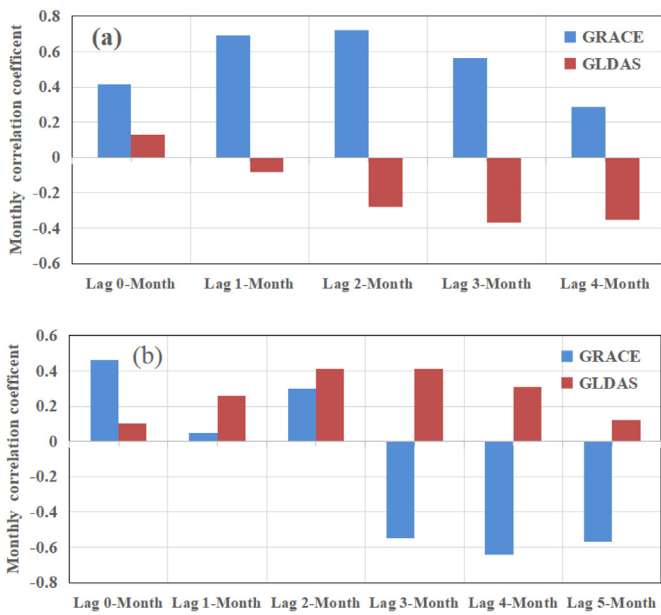

Fig. 9. The monthly hydrological correlation with varying length of time-lag periods ((a) between precipitation and GRACE-TWS change, GLDAS-SM change; (b) between P-ET and GRACE-TWS change, GLDAS-SM change).

regional aquitard, permafrost affected the spatial-temporal hydraulic connection between the groundwater and surface water, and it played a decisive role in the formation of groundwater, the transport processes, and the pattern of distribution of groundwater and its pathways (Lemieux et al., 2008; Woo et al., 2008). Thin permafrost had greater impacts on ice formation during the freezing season and greater impacts on the baseflows during the thawing season, and the mutual influences of groundwater and surface waters were significant in the permafrost regions (Zhang et al., 2008; Gao et al., 2016; Qin et al., 2017). The active soil thawing in the upper 60-cm soil contributed to the increase in discharge; however, the increase in thawing depth in soil layers deeper than 60 cm led to a decrease in surface runoff and slowed in the recession process (Wang et al., 2009). The supra-permafrost groundwater discharge decreased exponentially with active layer frozen processes during autumn runoff recession; in contrast, the ratio of groundwater discharge to total discharge and the direct surface discharge coefficient simultaneously increased (Wang et al., 2012, 2017). Ground warming led to higher permeability and wetter aquifers in the permafrost. The increase and thickening of the active layer could lead to the greater infiltration of surface water into the groundwater, resulting in increased water storage.

On the other hand, there are numerous and large thawed ponds, lakes, and drained thawed-lake basins in the TRSR (Lei et al., 2014). These lakes mainly reside in the thick ice-rich continuous permafrost zone (Fig. 1). The development and growth of lakes is related to the
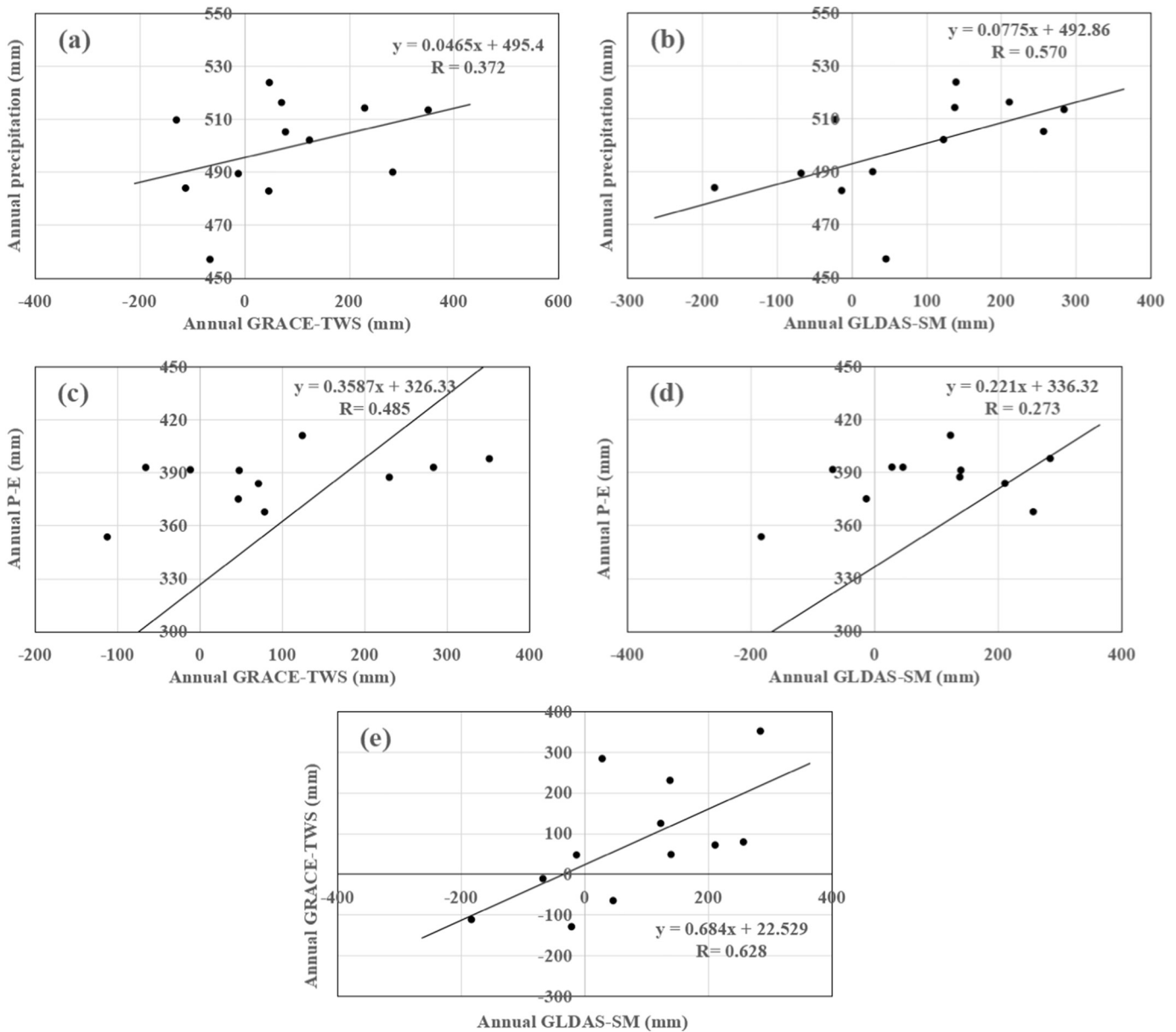
Fig. 10. The correlation between annual hydrological variables.

thermal processes that occur at the ice-wedge intersections, the permafrost thawing with subsidence of the ground surface, and the increased thickness of the active layer (Muskett and Romanovsky, 2011). Over time, small ponds have merged into large lakes and some drained when thermo-erosion and bank undercutting caused a breach (Hinkel et al., 2003, 2005). Beneath such lakes, the talik that was previously unfrozen soil developed into a closed talik, and the lateral and vertical extents of a talik depend on the internal structure of the permafrost and on

the temperature regime at the ground surface (Yoshikawa and Hinzman, 2003). Eventually, the talik became an open talik and served as an aquifer, whereby lake water drained and became subsurface groundwater; this process increased the water storage within or in some cases below the permafrost. This indicated that surface water was being recruited for subsurface groundwater storage and that the groundwater residence time was increasing. Additionally, water storage increased, and this was supported by the increase in the number and area of thawed bogs, ponds, and lakes. Research has indicated that the number of lakes has been increasing in the continuous permafrost zone in the study area (Lei et al., 2014). The findings of the present study regarding GW changes in the TRSR during 2003–2014 are consistent with these observations.

6. Conclusions

In this study, the hydrological variations and their impacts on vegetation were investigated in the TRSR during the period of 2003–2014. The main conclusions are as follows:

Table 1
Relationships between NDVI of growing season and seasonal temperature and hydrological variables in the TRSR.

		Spring	Summer	Autumn	Winter	Annual
Growing season NDVI	Temperature	0.226	0.671[**]	0.127	0.001	0.415
	Precipitation	0.672[**]	0.422	0.213	0.220	0.567[*]
	ET	0.450	0.087	0.039	0.039	0.240
	GRACE-TWS	0.552[*]	0.545[*]	0.384	0.750[**]	0.638[**]
	GLDAS-SM	0.614[*]	0.726[**]	0.440	0.674[**]	0.692[**]

[*] 95% confidence level.
[**] 99% confidence level.

(1) The precipitation showed an increasing trend at a rate of 14.0 mm 10 a^{-1}, and ET showed a slight decreasing trend. The GRACE-TWS variations presented an increasing trend at a rate of 35.1 mm a^{-1}, and the GW change showed an increasing trend at a rate of 18.5 mm a^{-1}. The hydrological cycle has obviously changed. More water was stored in the TRSR, and more soil water has been transported into GW since the aquiclude changed. More precipitation would lead to more GRACE-TWS changes when precipitation preceded GRACE-TWS changes by 2 months, it would induce less GLDAS-SM change when precipitation preceded it by 3 months. The time lag of the GRACE-TWS change that was influenced by precipitation was more obvious than that of the GLDAS-SM change. No consistent changes in the correlation between the hydrological variables were found with the increase in the time-lag.

(2) The annual precipitation had the greatest impact on the surface water (GLDAS-SM). The annual precipitation and ET affected the total water storage change (GRACE-TWS) which also responded to GLDAS-SM change in the TRSR. Precipitation was relatively lower in winter and spring, and the water flow out of the TRSR was predominantly in the forms of ET and discharge which led the TWS in a state of loss. The GRACE-TWS change was generally higher in summer and autumn and lower in winter and spring. The water was mainly stored as SM from January to July, and it was stored as GW from July to December in the TRSR. The spatial distribution of ET was consistent with that of precipitation. The distribution of TWS change was not only influenced by precipitation, but also may be affected by the type of the underlying surface (permafrost and lakes).

(3) The vegetation in the TRSR was greening between 2003 and 2014. The spatial distribution of the NDVI was seen to be quite relative in terms of the climate and hydrological variations. The trend of the NDVI indicated that 90% of the TRSR areas had a positive annual variation rate, while the negative rate found in the other areas corresponded to degraded vegetation. The areas where vegetation was worsening were located in parts of the eastern, southern, and western TRSR. Spring precipitation and summer temperature were the conditions that limited the growth of vegetation growth, and that precipitation was more important than temperature. However, the effect of the total TWS change and GLDAS-SM change on vegetation was considerably greater than the effects of other factors in this region.

(4) As a special regional aquitard, ground warming led to higher permeability and wetter aquifers in the permafrost of the TRSR. Permafrost affected the spatial-temporal hydraulic connection between the groundwater and surface water, and it played a decisive role in the formation of groundwater, the transport processes, and the pattern of distribution of groundwater and its pathways. The increase and thickening of the active layer can lead to the greater infiltration of surface water into the groundwater, which can result in increased water storage. On the other hand, water storage may have increased due to the increase in the number and area of thawed bogs, ponds, and lakes in the study area. The GRACE-TWS data can be used to investigate the effects of permafrost on hydrology over the cold regions under the influence of climate change.

The TWS change, including surface water, snow and ice, soil moisture, and groundwater, is essential for understanding a wide range of hydrological, climatological, and ecological processes and it is important for water resource management. In situ monitoring of regional-scale TWS change is extremely limited, especially in remote alpine areas. Traditional remote sensing satellites and models can be used to detect or simulated surface soil moisture to depths of only tens of centimeters, and the spatial distribution of field stations for verification purposes is poor. However, the GRACE satellite can compensate for such disadvantages. The GRACE-derived TWS change considers all hydrological components for regional-to-global coverage, which offers a new opportunity for understanding of regional hydrology, especially interactions and impacts of hydrological changes.

Acknowledgement

References

Cao, Y., Nan, Z., Cheng, G., 2015. GRACE gravity satellite observations of terrestrial water storage changes for drought characterization in the arid land of northwestern China. Remote Sens. 7 (1), 1021–1047.

Chen, J., Li, J., Zhang, Z., Ni, S., 2014b. Long-term groundwater variations in northwest India from satellite gravity measurements. Glob. Planet. Chang. 116 (1), 130–138.

Chen, T., de Jeu, R.A.M., Liu, Y.Y., van der Werf, G.R., Dolman, A.J., 2014a. Using satellite based soil moisture to quantify the water driven variability in NDVI: a case study over mainland Australia. Remote Sens. Environ. 140, 330–338.

Chen, X., Su, Z.B., Ma, Y.M., James, C., Michael, L., 2017. An accurate estimate of monthly mean land surface temperatures from MODIS clear-sky retrievals. J. Hydrometeorol. 18 (10), 2827–2847.

Chen, X., Su, Z.B., Ma, Y.M., Liu, S.M., Yu, Q., Xu, Z., 2014c. Development of a 10-year (2001−2010) 0.1° data set of land-surface energy balance for mainland China. Atmos. Chem. Phys. 14 (23), 13097–13117.

Chen, X., Su, Z.B., Ma, Y.M., Yang, K., Wen, J., Zhang, Y., 2013. An improvement of roughness height parameterization of the Surface Energy Balance System (SEBS) over the Tibetan Plateau. J. Appl. Meteorol. Climatol. 52 (3), 607–622.

Cheng, G., Jin, H., 2013. Permafrost and groundwater on the Qinghai-Tibet plateau and in northeast China. Hydrogeol. J. 21 (1), 5–23.

Cheng, M.K., Ries, J.C., Tapley, B.D., 2011. Variations of the Earth's figure axis from satellite laser ranging and GRACE. J. Geophys. Res. 116, B01409.

Deng, H., Chen, Y., 2016. Influences of recent climate change and human activities on water storage variations in central Asia. J. Hydrol. 544, 46–57.

Feng, W., Zhong, M., Lemoine, J.M., Biancale, R., Hsu, H.T., Xia, J., 2013. Evaluation of groundwater depletion in North China using the Gravity Recovery and Climate Experiment (GRACE) data and ground-based measurements. Water Resour. Res. 49, 2110–2118.

Gao, J., Zhang, Y., Liu, L., Wang, Z., 2014. Climate change as the major driver of alpine grasslands expansion and contraction: a case study in the Mt. Qomolangma (Everest) National Nature Preserve, southern Tibetan Plateau. Quat. Int. 336, 108–116.

Gao, T., Zhang, T., Lin, C., Kang, S., Sillanpää, M., 2016. Reduced winter runoff in a mountainous permafrost region in the northern Tibetan Plateau. Cold Reg. Sci. Technol. 126, 36–43.

Gao, Y., Zhou, X., Wang, Q., Wang, C., Zhan, Z., Chen, L., 2013. Vegetation net primary productivity and its response to climate change during 2001–2008 in the Tibetan Plateau. Sci. Total Environ. 444 (444), 356–362.

Geruo, A., Wahr, J., Zhong, S., 2013. Computations of the viscoelastic response of a 3-d compressible earth to surface loading: an application to glacial isostatic adjustment in Antarctica and Canada. Geophys. J. Int. 192 (2), 557–572.

Hinkel, K.M., Eisner, W.R., Bockheim, J.G., Nelson, F.E., Peterson, K.M., Dai, X., 2003. Spatial extent, age, and carbon stocks in drained thaw lake basins on the barrow peninsula, Alaska. Arct. Antarct. Alp. Res. 35 (3), 291–300.

Hinkel, K.M., Frohn, R.C., Nelson, F.E., Eisner, W.R., Beck, R.A., 2005. Morphometric and spatial analysis of thaw lakes and drained thaw lake basins in the western Arctic coastal plain, Alaska. Permafr. Periglac. Process. 16 (4), 327–341.

Hu, M.Q., Mao, F., Sun, H., Hou, Y.Y., 2011. Study of normalized difference vegetation index variation and its correlation with climate factors in the Three-River-Source Region. Int. J. Appl. Earth Obs. Geoinf. 13 (1), 24–33.

Huntington, T.G., 2006. Evidence for intensification of the global water cycle: review and synthesis. J. Hydrol. 319 (1–4), 83–95.

Immerzeel, W.W., van Beek, L.P., Bierkens, M.F., 2010. Climate change will affect the Asian water towers. Science 328, 1382–1385.

Jennifer, R., Lei, J., Bruce, K., Wylie, L. Tieszen, 2012. Establishing water body areal extent trends in interior Alaska from multi-temporal Landsat data. Remote Sens. Lett. 3 (7), 595–604.

Jin, S., Feng, G., 2013. Large-scale variations of global groundwater from satellite gravimetry and hydrological models, 2002–2012. Glob. Planet. Chang. 106 (3), 20–30.

Kang, S., Xu, Y., You, Q., Flügel, W., Pepin, N., Yao, T., 2010. Review of climate and cryospheric change in the Tibetan Plateau. Environ. Res. Lett. 5, 015101.

Landerer, F.W., Swenson, S.C., 2012. Accuracy of scaled GRACE terrestrial water storage estimates. Water Resour. Res. 48 (4), 4531.

Lei, Y., Yang, K., Wang, B., Sheng, Y., Bird, B.W., Zhang, G., 2014. Response of inland lake dynamics over the Tibetan Plateau to climate change. Clim. Chang. 125 (2), 281–290.

Lemieux, J.M., Sudicky, E.A., Peltier, W.R., Tarasov, L., 2008. Dynamics of groundwater recharge and seepage over the Canadian landscape during the Wisconsinian glaciation. J. Geophys. Res. 113, F01011.

Lewis, S.L., Brando, P.M., Phillips, O.L., van der Heijden, G.M., Nepstad, D., 2011. The 2010 Amazon drought. Science 331, 554.

Liang, L.Q., Li, L.J., Liu, C.M., Cuo, L., 2013. Climate change in the Tibetan Plateau three rivers source region: 1960–2009. Int. J. Climatol. 33 (13), 2900–2916.

Long, D., Chen, X., Scanlon, B.R., Wada, Y., Hong, Y., Singh, V.P., Chen, Y., Wang, C., Han, Z., Yang, W., 2016. Have GRACE satellites overestimated groundwater depletion in the Northwest India aquifer? Sci. Rep. 6, 24398.

Luo, S., Fang, X., Lu, S., Ma, D., Chang, Y., Song, M., 2016. Frozen ground temperature trends associated with climate change in the Tibetan Plateau Three River Source Region from 1980 to 2014. Clim. Res. 67(3).

Muskett, R.R., Romanovsky, V.E., 2011. Alaskan permafrost groundwater storage changes derived from GRACE and ground measurements. Remote Sens. 3 (2), 378–397.

Piao, S., Tan, K., Nan, H., Ciais, P., Fang, J., Wang, T., 2012. Impacts of climate and CO_2 changes on the vegetation growth and carbon balance of Qinghai-Tibetan grasslands over the past five decades. Glob. Planet. Chang. 98–99 (6), 73–80.

Qin, Y., Yang, D., Gao, B., Wang, T., Chen, J., Chen, Y., Wang, Y.H., Zheng, G.H., 2017. Impacts of climate warming on the frozen ground and eco-hydrology in the Yellow River source region. China. Sci. Total Environ. 605–606, 830.

Roach, J., Griffith, B., Verbyla, D., Jones, J., 2011. Mechanisms influencing changes in lake area in Alaskan boreal forest. Glob. Planet. Chang. 17 (8), 2567–2583.

Rodell, M., Famiglietti, J.S., Chen, J., Seneviratne, S.I., Viterbo, P., Holl, S., Wilson, C.R., 2004. Basin scale estimates of evapotranspiration using GRACE and other observations. Geophys. Res. Lett. 31 (20), 183–213.

Rodell, M., Velicogna, I., Famiglietti, J., 2009. Satellite-based estimates of groundwater depletion in India. Nature 460, 999–1002.

Shen, M., Piao, S., Jeong, S.J., Zhou, L., Zeng, Z., Ciaisf, P., Cheng, D., Huangc, M., Jinh, C.S., Li, L.Z., Li, Y., Myneni, R.B., Yang, K., Zhang, G., Zhang, Y., Yao, T., 2015. Evaporative cooling over the Tibetan Plateau induced by vegetation growth. P. Natl. Acad. of Sci. USA. 112, 9299–9304.

Solano, R., Didan, K., Jacobson, A., Huete, A., 2010. MODIS Vegetation Index User's Guide (MOD13 Series), Version 2.00, May 2010 (Collection 5). Vegetation Index and Phenology Lab, The University of Arizona.

Song, Y., Jin, L., Wang, H.B., 2018. Vegetation changes along the Qinghai-Tibet Plateau engineering corridor since 2000 induced by climate change and human activities. Remote Sens. 10 (1), 95.

Strassberg, G., Scanlon, B.R., Rodell, M., 2014. Comparison of seasonal terrestrial water storage variations from GRACE with groundwater-level measurements from the high plains aquifer (USA). Geophys. Res. Lett. 34 (14).

Su, Z., 2002. The Surface Energy Balance System (SEBS) for estimation of turbulent heat fluxes. Hydrol. Earth Syst. Sci. 6 (1), 85–99.

Swenson, S.C., Wahr, J., 2006. Post-processing removal of correlated errors in GRACE data. Geophys. Res. Lett. 33, L08402.

Syed, T.H., Famiglietti, J.S., Rodell, M., Chen, J., Wilson, C.R., 2008. Analysis of terrestrial water storage changes from GRACE and GLDAS. Water Resour. Res. 44 (2), W02433.

Thompson, S.E., Harman, C.J., Troch, P.A., Brooks, P.D., Sivapalan, M., 2011. Spatial scale dependence of ecohydrologically mediated water balance partitioning: a synthesis framework for catchment ecohydrology. Water Resour. Res. 47, W00J03.

Walvoord, M.A., Voss, C.I., Wellman, T.P., 2012. Influence of permafrost distribution on groundwater flow in the context of climate-driven permafrost thaw: example from Yukon flats basin, Alaska, United States. Water Resour. Res. 48 (7), 7524.

Wang, G., Hu, H., Li, T., 2009. The influence of freeze–thaw cycles of active soil layer on surface runoff in a permafrost watershed. J. Hydrol. 375 (3), 438–449.

Wang, G., Liu, G., Liu, L., 2012. Spatial scale effect on seasonal streamflows in permafrost catchments on the Qinghai-Tibet plateau. Hydrol. Process. 26 (7), 973–984.

Wang, G., Mao, T., Chang, J., Song, C., Huang, K., 2017. Processes of runoff generation operating during the spring and autumn seasons in a permafrost catchment on semi-arid plateaus. J. Hydrol. 550, 307–317.

Wang, J., Ye, B., Liu, F., Li, J., Yang, G., 2011. Variations of NDVI over elevational zones during the past two decades and climatic controls in the Qilian mountains, northwestern China. Arct. Antarct. Alp. Res. 43 (1), 127–136.

Wang, Q., Wang, J., Zhao, Y., Li, H., Zhai, J., Yu, Z., 2016a. Reference evapotranspiration trends from 1980 to 2012 and their attribution to meteorological drivers in the Three-River Source Region, China. Int. J. Climatol. 36 (11), 3759–3769.

Wang, X., Yi, S., Wu, Q., Yang, K., Ding, Y., 2016b. The role of permafrost and soil water in distribution of alpine grassland and its NDVI dynamics on the Qinghai-Tibetan plateau. Glob. Planet. Chang. 147, 40–53.

White, D., Hinzman, L., Alessa, L., Cassano, J., Chambers, M., Falkner, K., 2007. The Arctic freshwater system: changes and impacts. J. Geophys. Res. 112 (G4), 310–317.

Woo, K., Kane, D., Carey, S., Yang, D., 2008. Progress in permafrost hydrology in the New Millennium. Permafr. Periglac. Process. 19, 237–254.

Xiao, R., He, X., Zhang, Y., Ferreira, V.G., Chang, L., 2015. Monitoring groundwater variations from satellite gravimetry and hydrological models: a comparison with in-situ measurements in the mid-Atlantic region of the United States. Remote Sens. 7 (1), 686–703.

Xu, M., Kang, S., Zhao, Q., Li, J., 2016. Terrestrial water storage changes of permafrost in the three-river source region of the Tibetan Plateau, China. Adv. Meteorol. 2016 (1), 1–13.

Xu, W., Gu, S., Zhao, X.Q., Xiao, J., Tang, Y., Fang, J., 2011. High positive correlation between soil temperature and NDVI from 1982 to 2006 in alpine meadow of the Three-River Source Region on the Qinghai-Tibetan plateau. Int. J. Appl. Earth Obs. Geoinf. 13 (4), 528–535.

Xue, B.L., Wang, L., Li, X., Yang, K., Chen, D., Sun, L., 2013. Evaluation of evapotranspiration estimates for two river basins on the Tibetan Plateau by a water balance method. J. Hydrol. 492 (492), 290–297.

Yang, D., Ye, B., Kane, D.L., 2004. Streamflow changes over Siberian Yenisei river basin. J. Hydrol. 296 (1), 59–80.

Yang, K., Zhou, D., Wu, B., Foken, T., Qin, J., Zhou, Z., 2011. Response of hydrological cycle to recent climate changes in the Tibetan Plateau. Clim. Chang. 109 (3–4), 517–534.

Yang, M., Nelson, F.E., Shiklomanov, N.I., Guo, D., Wan, G., 2010. Permafrost degradation and its environmental effects on the Tibetan Plateau: a review of recent research. Earth-Sci. Rev. 103 (1–2), 31–44.

Yang, T., Wang, C., Yu, Z., Xu, F., 2013. Characterization of spatio-temporal patterns for various GRACE- and GLDAS-born estimates for changes of global terrestrial water storage. Glob. Planet. Chang. 109 (4), 30–37.

Ye, B., Yang, D., Ma, L., 2012. Effect of precipitation bias correction on water budget calculation in Upper Yellow River, China. Environ. Res. Lett. 7 (2), 25201–25210.

Ye, B., Yang, D., Zhang, Z., Kane, D.L., 2009. Variation of hydrological regime with permafrost coverage over Lena basin in Siberia. J. Geophys. Res. 114, D07102.

Yoshikawa, K., Hinzman, L.D., 2003. Shrinking thermokarst ponds and groundwater dynamics in discontinuous permafrost near council, Alaska. Permafr. Periglac. Process. 14 (2), 151–160.

Zhang, G., Yao, T., Shum, C.K., Yi, S., Yang, K., Xie, H., 2017. Lake volume and groundwater storage variations in Tibetan Plateau's endorheic basin. Geophys. Res. Lett. 44, 5550–5560.

Zhang, S., Hua, D., Meng, X., Zhang, Y., 2011. Climate change and its driving effect on the runoff in the Three-River headwaters region. J. Geogr. Sci. 21, 963–978.

Zhang, S., Liu, C., Yao, Z., Guo, L., 2010. Experimental study on lag time for a small watershed. Hydrol. Process. 21 (8), 1045–1054.

Zhang, W., Yi, Y., Song, K., Kimball, J., Lu, Q., 2016a. Hydrological response of alpine wetlands to climate warming in the eastern Tibetan Plateau. Remote Sens. 8 (4), 336.

Zhang, Y., Chen, W., Riseborough, D.W., 2008. Transient projections of permafrost distribution in Canada during the 21st century under scenarios of climate change. Glob. Planet. Chang. 60 (3), 443–456.

Zhang, Y., Zhang, C., Wang, Z., Chen, Y., Gang, C., An, R., Li, J.L., 2016b. Vegetation dynamics and its driving forces from climate change and human activities in the Three-River Source Region, China from 1982 to 2012. Sci. Total Environ. 563–564, 210–220.